Available online at www.sciencedirect.com
ScienceDirect
International Journal of Thermal Sciences 47 (2008) 1284–1293
International Journal of Thermal Sciences
www.elsevier.com/locate/ijts

Thermal state of an incompressible pseudo-plastic fluid and Nusselt number at the interface fluid–die wall

Mustapha Karkri [a,*], Yvon Jarny [b], Pierre Mousseau [c]

[a] *CERTES EA 3481 – Université Paris 12 Val de Marne, 94010 Créteil cedex, France*
[b] *UMR CNRS 6607 Ecole Polytechnique de l'Université de Nantes 44306 cedex, France*
[c] *UMR CNRS 6144 IUT – Université de Nantes, BP 539, 44475, France*

Received 7 February 2007; received in revised form 13 November 2007; accepted 24 November 2007

Available online 3 January 2008

Abstract

An experimental and numerical study was made of the steady laminar convective heat transfer to polyethylene Dowlex 2042E described by the Cross model flowing through an extrusion die. The inverse heat transfer problem is formulated to reconstruct the thermal history of the melted polymer in the channel die. Local Nusselt number distributions are presented for different flow rate and thermal boundary conditions. The effect of viscous dissipation combined with the flow rate on heat transfer is discussed. It is shown that an increasing flow rate leads to different Nusselt number and correlation is proposed to compute the heat transfer.

Keywords: Nusselt number; Extrusion die; Flow rate; Heat transfer

1. Introduction

In this work, the resolution of an inverse heat convection–conduction problem is developed to estimate the temperature field within the polymer flow from temperature measurements taken inside the die wall. The solution is computed according to the classical Conjugate Gradient Method (CGM).

The modeling equations for the fluid flow in the channel as well as for the heat flow within the melted polymer and the wall regions are solved simultaneously. The melted polymer is considered as an incompressible pseudo-plastic fluid and the flow is assumed steady and laminar. During polymer extrusion, even after the melting zone, heat transfer takes an important place at the outlet of the extruder [1,2]. The die has to be able to withstand the high temperatures and pressures exerted on it from the polymer being forced through it. It is recognized that under certain conditions, the release of heat resulting from viscous dissipation within a polymer flow is the source of heterogeneity of temperature within the fluid. Due to high viscous dissipation and very low heat conductivity, the temperature profile can be quite sharp. Overheated area can be generated within the flow and degradation of the polymer could occur. For such creeping flow the temperature field is affected far downstream from the die entrance, so to predict accurately and to control the temperature rise, the inlet temperature profile has to be taken into account. However, due to the history in the extruder, the material temperature at the die entrance is rarely uniform. Hence, the determination of this temperature profile is referred to as a boundary inverse heat transfer problem. There are numerous works on the initial temperature profile restoration, for example, [3] estimate the inlet temperature profile in the laminar duct flow and subsequent investigations [4–6] examine various aspects of this problem. Recently, Hsu et al. [7] presented a two-dimensional inverse least squares method to estimate both inlet temperature and wall heat flux in a steady laminar flow in a circular duct. Huang and Chen [8] have solved a non-stationary Navier–Stokes equation, to provide coefficients for energy equation, but the velocity field does not depend on temperature. Gejadze and Jarny [9] have presented a detailed analysis of an inverse heat transfer problem, when the velocity field depends on temperature field through viscosity for a non-Newtonian fluid. Recently, Nguyen and Prystay [10] esti-

* Corresponding author. Tel.: (+33) 1 45 18 36; fax: (+33) 01 45 17 65 51.
E-mail address: mustapha.karkri@univ-paris12.fr (M. Karkri).

1290-0729/$ – see front matter
doi:10.1016/j.ijthermalsci.2007.11.009

Nomenclature

C_p	heat capacity	$J\,kg^{-1}\,K$
D_h	hydraulic diameter	m
F	source term of energy	$Pa\,s^{-3}$
J	functional to be minimized	$°C^2$
L_{hp}	length of the heating plate	m
l_c	length of the die connector	m
P	pressure	Pa
Q	flow rate	$g\,s^{-1}$
T	temperature	°C
U	velocity	$m\,s^{-1}$
u, v	axial and radial velocities	$m\,s^{-1}$
u_m	mean velocity	$m\,s^{-1}$
$\tilde{Y}$	measured temperatures	°C

Greek symbols

$\dot{\gamma}$	shear rate	s^{-2}
η	dynamic viscosity	$Pa\,s^{-1}$
λ	conductivity	$W\,m^{-1}\,°C^{-1}$
α	perimeter	m
ρ	density	$kg\,m^{-3}$
Ω	spatial domain	
Ψ	adjoint variable	
θ	sensitivity variable	
δ	Dirac delta function	
∇	gradient	
∇	divergence	
Δ	Laplace	

Subscripts and superscripts

amb	ambient temperature
c	connector
m, p	sensor locations
m	mean temperature
0	inlet extrusion die
hp	heating plate
n	vector normal
p	polymer
s	outlet extrusion die
w	die wall

Definitions of non-dimensional variables

Nu	Nusselt number
Ca	Cameron number
P_e	Peclet number
Gz	Graetz number

mated the initial temperature profile and its evolution in polymer processing using the surface temperature measurement and the conjugate gradient method was employed to search for the minimum of the functional. The results of the inverse problem are used to study the influences of flow rates and viscous dissipation on convective laminar heat transfer at polymer/wall interface. A Nusselt number, appropriate for forced convection in plate die, is introduced and evaluated for various flow rates with non-uniform inlet temperature profile and symmetric boundary conditions. Due to the broad range of application of extrusion, several experimental and modeling works have been performed in order to understand the thermal state and rheological behaviour of polymer flow. In fact, many studies involving die flows in the existing literature have not neglected the effect of viscous dissipation, because the shear stress can induce a considerable power generation. However, in the existing convective heat transfer literature, this effect is usually regarded as important in flow of very viscous fluid and flow in capillary tubes [11–13]. For polymer (high viscosity and low thermal conductivity), the disregard of viscous dissipation can cause appreciable errors in the temperature distributions and local Nusselt number. It is desirable to have methods to calculate reliably Nusselt number for pseudo-plastic polymers flowing in different types of channel. This would facilitate the design and optimization of heat transfer equipment encountered in polymer processing. Shah and London [14], Shah and Bhatti [15] and Hartnett and Kostic [16] have reviewed the most important investigations available in the literature on convection in rectangular ducts. Gao and Hartnett [17] obtained a general expression of the fully developed Nusselt number for eight different combinations of uniformly heated and adiabatic duct walls. Barletta and Zanchini [18] studied the effect of viscous dissipation in the thermal entrance region of slug flow in a circular duct. The temperature field and the local Nusselt number were determined analytically for any prescribed axial distribution of wall heat flux including uniform, linearly varying and exponentially varying heat fluxes. This paper deals with the study of thermal history of the melted polymer in the channel die and the influence of the extrusion parameters on the local Nusselt number at the polymer/die interface.

2. Experimental details

2.1. Rheological properties

The sample material used in this work is a low-density polyethylene (LDPE Dowlex 2042^E extrusion grade) suitable for the production of blown film. We measure the shear viscosity of PE using two types of apparatus: capillary rheometer (Ceast Co., Italy) and Rubber Process Analyser (RPA 2000). The viscosity function $\eta(T(x,z),\dot{\gamma})$ is temperature and shear-rate dependent. The rheological properties were measured over the 450–510 K temperature range with shear rates varying from 0.1 to 1000 s^{-1}. Fig. 1 presents the melt flow curves at various temperatures. The shear viscosity decreases with increasing apparent shear rate. With a rise of temperature, the value of shear viscosity decreases, especially at low apparent shear rate. Determination of the viscosity curve, Fig. 1 over a wide range of shear rate values is essential for solving the flow: Eqs. (3)–(7). The data measurements were fitted (inverse method) to the

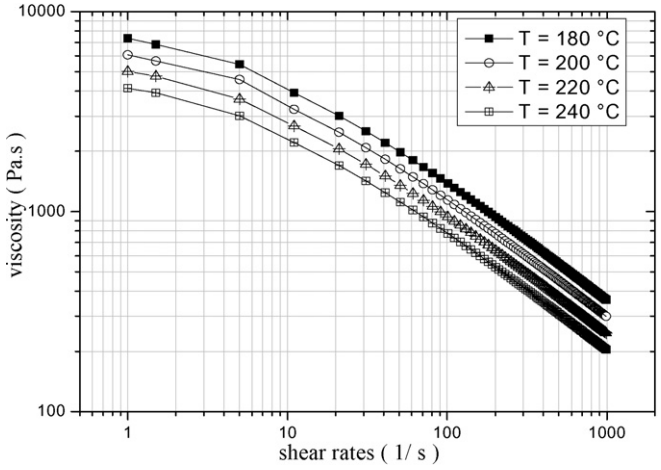

Fig. 1. Shear viscosity vs. shear rates for PE melt at various temperature.

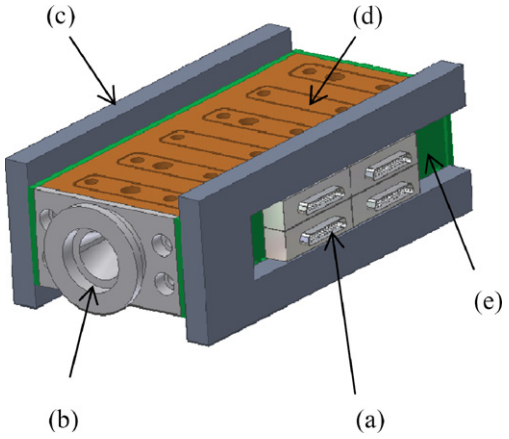

Fig. 2. Extrusion die (model 3D). (a) Thermocouple connectors, (b) inlet of the die (c) insulator, (d) heating plate, (e) composite material: polystyrene.

Cross model (Eq. (1)). Thermal conductivity of materials is measured under molding conditions (high pressure and high temperature) using an experimental apparatus coupled with inverse method [19]. The heat capacity $C_{pp}(T)$ was measured with a differential scanning calorimeter (Pyris 6 DSC), Eq. (2).

$$\eta(T,\dot{\gamma}) = K(T)/\left[1+(\lambda\dot{\gamma})^{1-n}\right], \quad K(T) = a\exp(bT) \tag{1}$$

where:

$$a = 54\,329\ \text{Pa s}, \quad b = -0.0095\ \text{K}^{-1}$$
$$\lambda = 0.16\ \text{s}^{-1} \quad \text{and} \quad n = 0.36$$
$$C_{pp}(T) = 2093.2 + 2.9059 \times T, \quad T \in [150\,^{\circ}\text{C}, 250\,^{\circ}\text{C}] \tag{2}$$

2.2. Extrusion die and methodology

The main parts of the experimental extrusion die, described in Figs. 2 and 3, are as follows: A rectangular channel (2×30 mm^2), is connected to the extruder outlet through a cone length of $l_c = 0.051$ m, the total channel length is $L_{ch} = 0.24$ m. The channel walls are made of four stainless blocks. The length, thickness and width of each block are $L = 0.2$ m, $H = 0.019$ m and $l_b = 0.05$ m. Two electrical heater plates ensure the heating of the die on the upper and the lower faces. To limit the heat side losses, two kinds of insulator are used: a composite material (thickness: 0.002 m) and a porous material (thickness: 0.03 m) surround the non-heated side surfaces of the extrusion die. The assumption of bi-dimensional heat transfer [11] enabled us to consider instrumentation in the median plane. Die wall temperatures were measured in several places by using 56 thermocouples type K: 24 thermocouples are located close to the upper and lower faces of the channel, 20 thermocouples close to both heating plates and 8 thermocouples are located at the outer face of the die. Dynisco Pressure Transducer is used to make pressure measurements of molten polymers

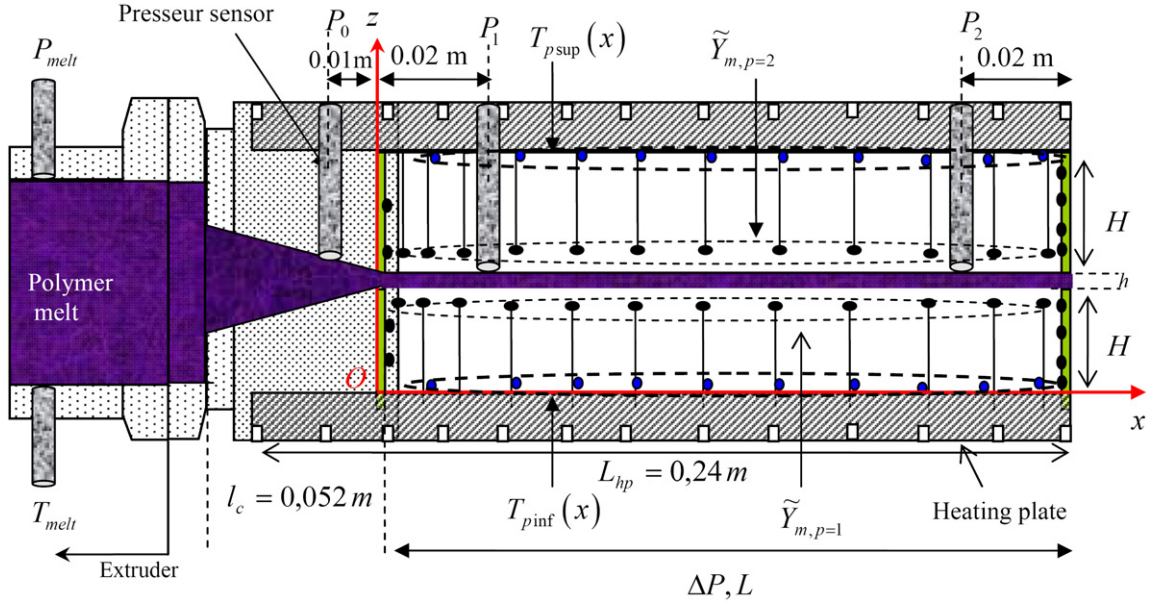

Fig. 3. Experimental die–sensor locations in x and z directions.

Table 1
Tests conditions of PE Dowlex 2042^{E}

Tests	Screw rotation (rpm)	T_{melt} (°C)	P_{melt} (MPa)	ΔP (MPa)	Q (g s^{-1})
1	10	201 ∓ 1	9.9	8.8	0.15
2	19	201 ∓ 1	15.6	13.9	0.29
3	26	202 ∓ 1	20	17.7	0.43
4	37	201 ∓ 1	25	21.3	0.53

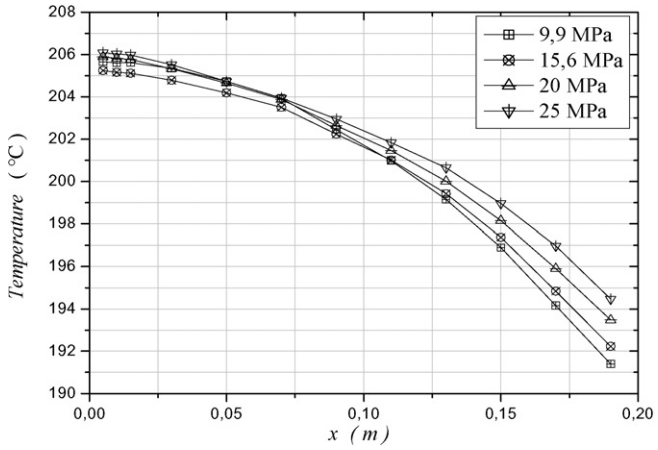

Fig. 4. Measured temperature $\tilde{Y}_{m,p}$ vs. pressure drop.

up to 400 °C. All the measurements were taken using a high-speed data acquisition system coupled to a personal computer and controlled by a VEE-Pro program. The pressure measurement is essential since it is boundary condition of the mathematical model (Eqs. (3)–(7)). The thermophysical properties of the metallic die are assumed constant ($\lambda_w = 16$ W mK^{-1}, $Cp_w = 400$ J kg^{-1} K).

2.3. Processing parameter

All the experiments were carried out with a single-screw extruder. The minimum and maximum flow rates are respectively 0.5 and 15 kg h^{-1}. Flow rate was measured by weighing the mass of polymer exiting the die with an electronic balance. The pressure drop (ΔP) along the channel die was also measured by using three pressure sensors located at $x = -0.01$ m, $x = 0.02$ m and $x = 0.18$ m. Several tests on the PE Dowlex 2042^{E} were carried out at different flow rates 0.29–0.53 g s^{-1}. Some experimental conditions are listed in Table 1. Figs. 4 and 5 show the temperature profiles measured within the die, both at the polymer/wall interface and at the heating-plates/wall interface. The temperature is maximal at the die inlet and then decreases slightly. At the die outlet, the temperature profiles near the channel increase with the flow rate. This observation is probably due to the shear heating effect.

3. Basic equations

3.1. Energy and momentum equations

Fig. 6 shows the 2-D geometrical model ($\Omega = \Omega_1 \cup \Omega_0$) of the extrusion die in a median plane parallel to the flow direction.

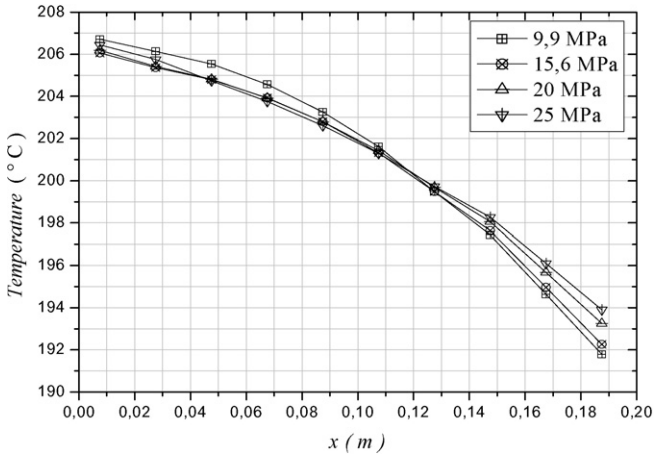

Fig. 5. Temperature near the heating-plate: $T_{p\,\sup,\inf}(x)$ (boundary condition of the model).

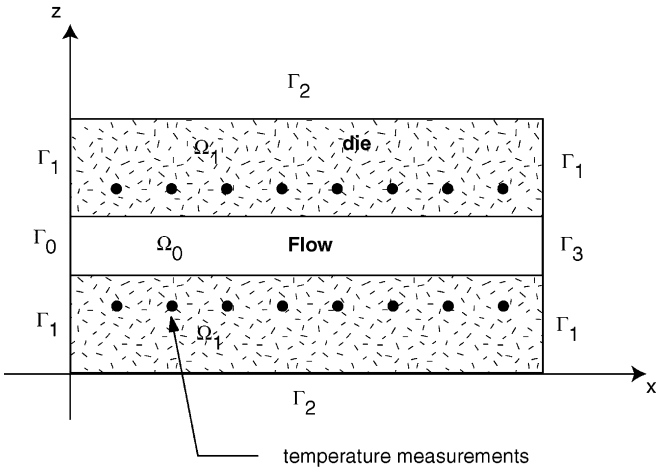

Fig. 6. Extrusion die/2-D spatial domain (median plan of the die).

The polymer melt enters the extrusion die at $x = 0$ with a temperature profile $T_0(z)$. The velocity and the temperature fields are governed by the coupled equations of mass, momentum and energy, i.e.

$$\nabla.U = 0 \quad \text{in } \Omega_0 \tag{3}$$

$$\rho_p\big(\nabla.(U \otimes U) - U\nabla.(U)\big) = -\nabla P + \nabla.\big(\eta(\nabla U + \nabla^t U)\big) \quad \text{in } \Omega_0 \tag{4}$$

$$\rho_p C_{pp}\big(\nabla.(UT) - T\nabla.U\big) = \nabla.(\lambda_p \nabla T) + F + S_p \quad \text{in } \Omega_0 \tag{5}$$

$$\nabla.(\lambda_w \nabla T) = S_w \quad \text{in } \Omega_1 \tag{6}$$

The term F is due to viscous dissipation, it is given by:

$$F = \eta \nabla U : \big(\nabla U + \nabla^t U\big) \tag{7}$$

The terms S_p and S_w are introduced for taking into account the heat losses through the connectors and the insulators of the non-heated side face of the experimental extrusion die.

$$S_{p,w}(x, z; T) = \chi^{\text{zone}} \Delta T = \frac{h_{\text{eq}}^{\text{zone}}}{l_b}\big[T(x, y) - T_{\text{amb}}\big]$$
$$(x, z) \in \Omega = [0, 0.2] \times [0, 0.04] \tag{8}$$

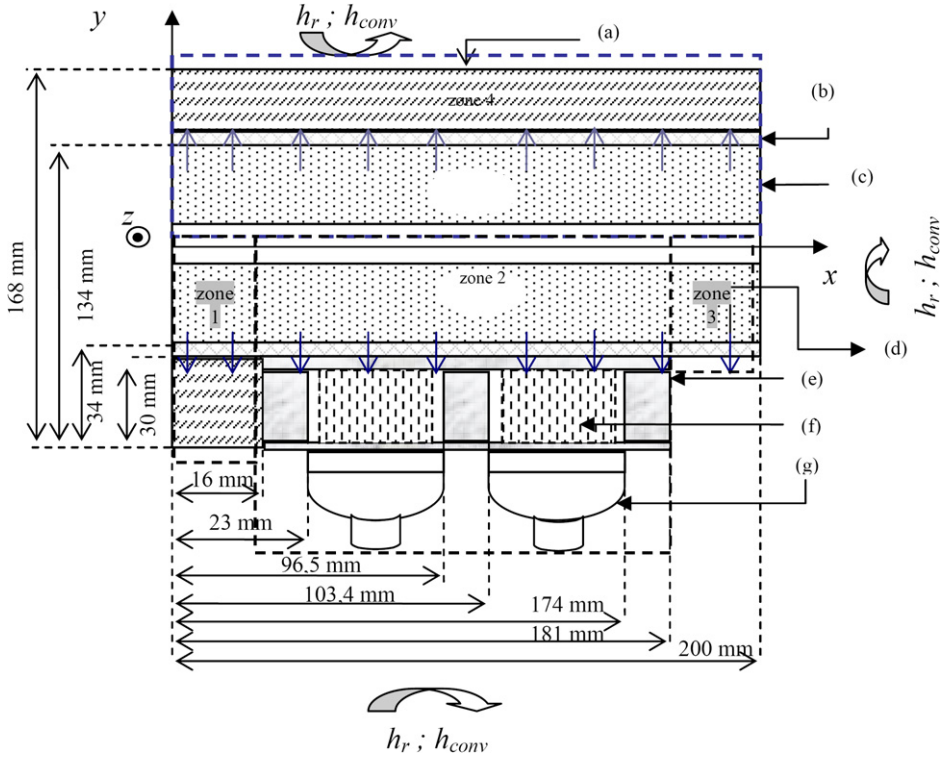

Fig. 7. (a) Insulator (foam glass), (b) insulator (polystyrene), (c) die wall, (d) heat flux from melted polymer to the connectors and insulators, (e) aluminum to fix the connectors, (f) thermocouples, (g) connectors.

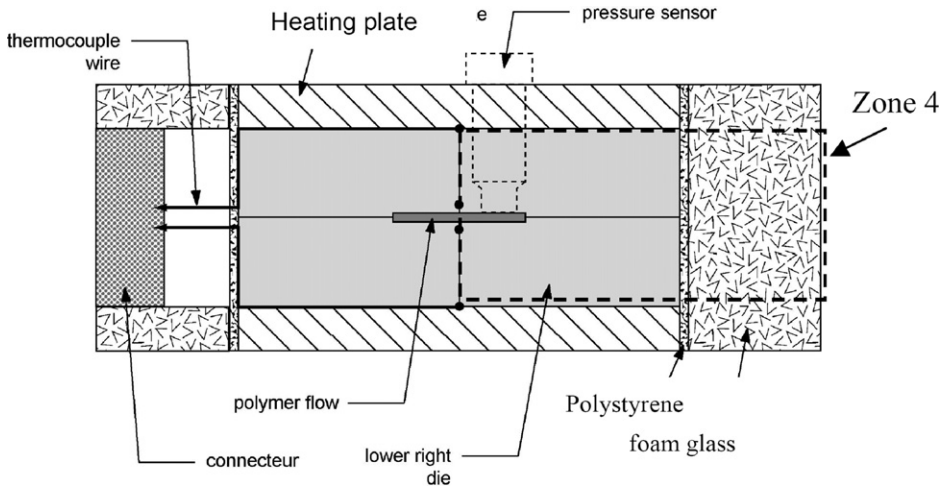

Fig. 8. Cross-section of the extrusion die: locations of heat losses zones.

where:

$$h_{\mathrm{eq}}^{\mathrm{zone}} = \lambda_w \sqrt{\frac{h_{\mathrm{ex}}\alpha}{\lambda_w S^{\mathrm{zone}}}} \left[\frac{\tanh\left(\sqrt{\frac{h_{\mathrm{ex}}\alpha}{\lambda_w S^{\mathrm{zone}}}} l_b\right) + \frac{h_{\mathrm{ex}}}{\lambda_w \sqrt{\frac{h_{\mathrm{ex}}\alpha}{\lambda_w S^{\mathrm{zone}}}}}}{1 + \frac{h_{\mathrm{ex}}}{\lambda_w \sqrt{\frac{h_{\mathrm{ex}}\alpha}{\lambda_w S^{\mathrm{zone}}}}} \tanh\left(\sqrt{\frac{h_{\mathrm{ex}}\alpha}{\lambda_w S^{\mathrm{zone}}}} l_b\right)} \right] \quad (9)$$

In order to determine the heat losses, the experimental extrusion die was divided in four zones as shown in Fig. 7. Each zone starts from the median plan of the extrusion die (Fig. 8) to the environment. The heat transfer coefficient for each zone is $h_{\mathrm{eq}}^{\mathrm{zone}}$, obtained by the thermal theory of the "rectangular fin" of uniform cross section in the width direction (Oy) [20], where α, l_b and S^{zone} are the perimeter, thickness and surface area of each zone (Table 2), respectively.

3.2. Boundary conditions

The following boundary conditions are considered for the velocity field:

– At the inlet of the channel:

$$P = P_0, \quad \frac{\partial u}{\partial x} = 0 \quad \text{and} \quad v = 0 \quad \text{on } \Gamma_0 \quad (10)$$

Table 2
Heat losses coefficients

Zones	h_{eq}^{zone} ($W\,m^{-2}\,K^{-1}$)	S^{zone} (m^2) $\times 10^{-6}$	α (m)	χ^{zone} ($W\,m^{-3}\,K^{-1}$)
1	6.51	640	0.112	130
2	87	6600	0.410	932
3	32	760	0.118	657
4	4.98	8000	0.48	99.65

– At the outlet of the channel:

$$P = P_s, \quad \frac{\partial^2 u}{\partial x^2} = 0 \quad \text{and} \quad \frac{\partial v}{\partial x} = 0 \quad \text{on } \Gamma_3 \tag{11}$$

– At the internal surface, the usual no-slip boundary condition is:

$$U = 0 \tag{12}$$

For the temperature field, the boundary conditions are taken as follows:

– At the channel entrance:

$$T = T_0(z) \quad \text{on } \Gamma_0 \tag{13}$$

The heat flux and the surface temperature of the die are fixed:

$$\lambda_p \frac{\partial T}{\partial n} = 0 \quad \text{on } \Gamma_3 \quad \text{and} \quad \lambda_w \frac{\partial T}{\partial n} = 0 \quad \text{on } \Gamma_1 \tag{14}$$

$$T = T_{p\,\sup,\inf}(x) \quad \text{on } \Gamma_2 \quad \text{and} \quad T = T_s(z) \quad \text{on } \Gamma_4 \tag{15}$$

4. Inverse heat transfer problem

The inlet temperature profile $T_0(z)$ has to be determined from the temperature $\tilde{Y}_{m,p}$ given by Ns sensors located inside the extrusion die at (x_m, z_p), $m = 1, \ldots, Ns/2$, $p = 1, 2$. The inverse problem is formulated by considering the following least square functional:

$$J(T_0) = \frac{1}{2} \sum_{p=1}^{2} \sum_{m=1}^{Ns/2} \left(T(x_m, z_p; T_0) - \tilde{Y}_{m,p}\right)^2 \tag{16}$$

where $T(x_m, z_p; T_0)$ are the temperature computed from the direct problem equations, at the measurement locations, with the estimated inlet temperature profile $T_0(z)$. The CGM was used to search for the minimum of the functional. This method has been well documented elsewhere [21,23] and will not be repeated here. The method is based on the computation of the gradient of the functional, which is obtained by solving the sensitivity problem and the adjoint problem defined as follows.

4.1. The sensitivity problem

In order to develop the sensitivity problem equations, a variation $\varepsilon\delta T_0$ of the inlet temperature profile is considered, and the resulting temperature is denoted $T(x, z; T_0 + \varepsilon\delta T_0)$. The sensitivity is then defined by:

$$\theta = \lim_{\varepsilon \to 0} \frac{T(x, z; T_0 + \varepsilon\delta T_0) - T(T_0)}{\varepsilon} = \lim_{\varepsilon \to 0} \frac{T^+ - T(T_0)}{\varepsilon} \tag{17}$$

Developing the direct problem (Eqs. (3)–(7)) for $T(x, z; T_0)$ and $T(x, z; T_0 + \varepsilon\delta T_0)$ and then subtracting the resulting expressions leads to:

$$\rho C_{pp} U.\nabla(\theta) = \nabla.(\lambda_p \nabla\theta) + \frac{\partial(F + S_p)}{\partial T}\theta \quad \text{in } \Omega_0 \tag{18}$$

$$\lambda_w \frac{\partial \theta}{\partial n} = 0 \quad \text{on } \Gamma_1 \quad \text{and} \quad \lambda_p \frac{\partial \theta}{\partial n} = 0 \quad \text{on } \Gamma_3 \tag{19}$$

$$\theta = 0 \quad \text{on } \Gamma_2, \Gamma_4 \quad \text{and} \quad \theta = \delta T_0 \quad \text{on } \Gamma_0 \tag{20}$$

$$\nabla.(\lambda_w \nabla\theta) = \frac{\partial S_w}{\partial T}\theta \quad \text{in } \Omega_1 \tag{21}$$

where U is the direct problem velocity profile in the extrusion die.

4.2. The adjoint problem

The following adjoint problem equations are obtained [20]:

$$\rho_p C_{pp} U \nabla(\psi) + \lambda_p \Delta\psi + \frac{\partial(F + S_p)}{\partial T}\psi = \sum_{p=1}^{2} \sum_{m=1}^{Ns/2} \left(T(x_m, z_p; T_0) - \tilde{Y}_{m,p}\right)\delta_{x_m}(x)\delta_{z_p}(z) \quad \text{in } \Omega_0 \tag{22}$$

$$\psi = 0 \quad \text{on } \Gamma_0 \quad \text{and} \quad \lambda_w \frac{\partial \psi}{\partial n} = 0 \quad \text{on } \Gamma_1 \tag{23}$$

$$\psi = 0 \quad \text{on } \Gamma_2, \Gamma_4 \quad \text{and}$$

$$\lambda_p \frac{\partial \psi}{\partial n} + \rho_p C_{pp} \vec{U}.\vec{n}\psi = 0 \quad \text{on } \Gamma_3 \tag{24}$$

$$\nabla.(\lambda_w \nabla\psi) = \frac{\partial S_w}{\partial T}\psi \quad \text{in } \Omega_1 \tag{25}$$

together with the gradient equation:

$$\nabla J(T_0) = \lambda_p \frac{\partial \psi}{\partial n}\bigg|_{\Gamma_0} \tag{26}$$

5. Results and discussion

5.1. Estimation of polyethylene inlet temperature profile

5.1.1. Effect of the heat losses

In this paragraph, we will show the influence of the thermal losses in (oy) direction through the non-heated side faces die, on the inlet-estimated temperature profile. Two solutions have been computed one with the heat losses $S_{p,w}(x, z; T)$ equal to zero, the other one where $S_{p,w}(x, z, T)$ is given by Eq. (8) [22].

5.1.1.1. Case I without heat losses: $S_{p,w}(x, z, T) = 0$. The computation starts from the uniform guess $T_0^{n=0}(z) = 197\,^{\circ}C$ and the boundary model conditions are shown on Figs. 5 and 9–10. In Fig. 11, comparison is made between the initial temperature profile and the reconstructed temperature profile for different flow rates. It can be observed that the temperature is

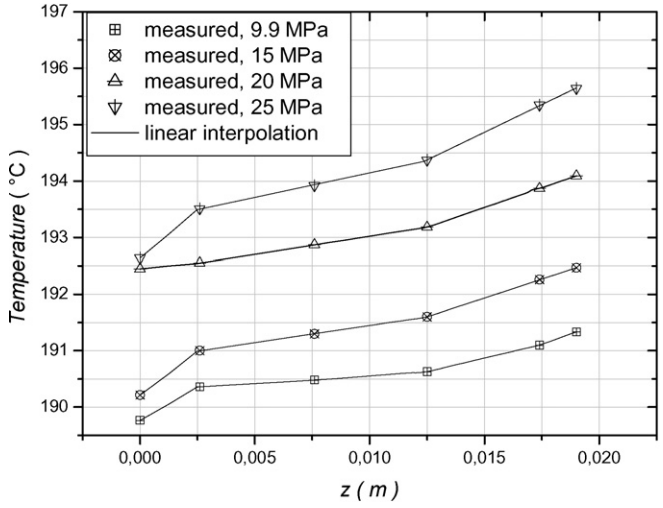

Fig. 9. Measured temperature at the outer die face T_s ($x = 200$ mm, $0 < z \leqslant 19$ mm).

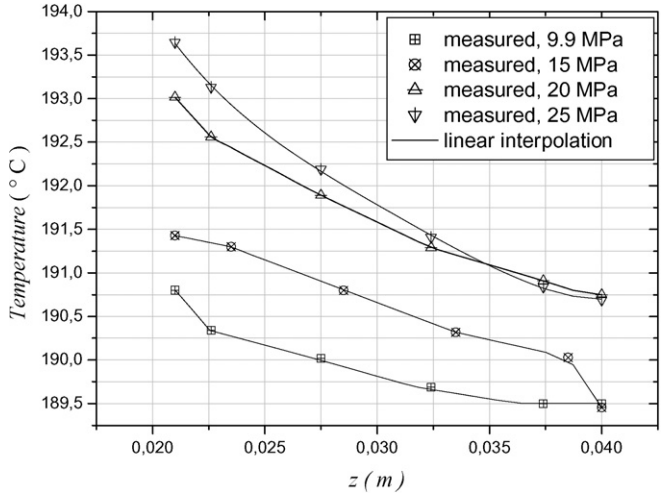

Fig. 10. Measured temperature at the outer die face T_s ($x = 200$ mm, 21 mm $< z \leqslant 40$ mm).

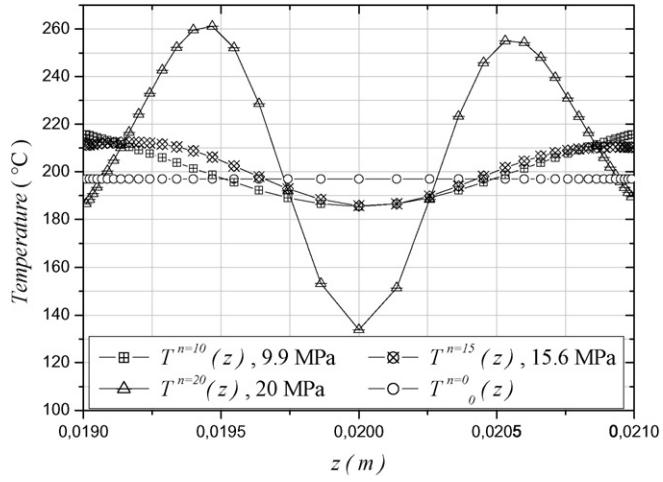

Fig. 11. Estimated inlet temperatures profile, $S_{p,w} = 0$.

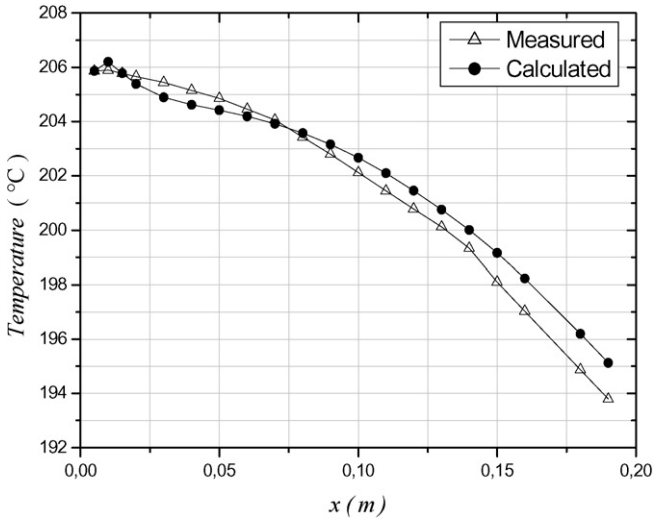

Fig. 12. Measured $\tilde{Y}_{m,p}$ and calculated temperatures, $P_{\text{melt}} = 20$ MPa, $S_{p,w} = 0$.

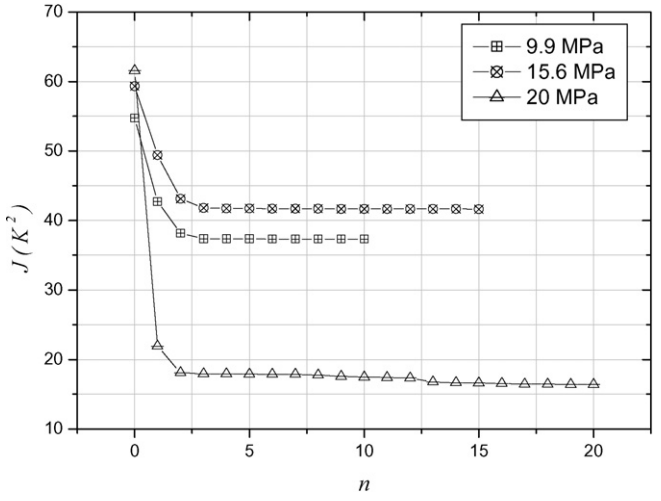

Fig. 13. Least square criterion $J(T_0(z))$, $S_{p,w} = 0$.

very high near the walls (188–260 °C) and low in the channel center (130–187 °C). The estimated profile is physically difficult to interpret. Figs. 12–13 show the comparison between the measured and calculated temperature at polymer-walls interfaces of PE and the evolution of the least square criterion for three operating conditions: 9.9–15.6 and 20 MPa. Because the least square criterion remains constant after three iterations, we are forced to consider that the mathematical model is not able to predict the real system exactly.

5.1.1.2. Case II with heat losses: ($S_{p,w}(x, z, T) \neq 0$). The computation starts from the uniform guess $T_0^{n=0}(z) = 197\,^{\circ}\text{C}$. In Fig. 14, comparison is made between the initial temperature profile and the reconstructed temperature profile. It can be observed that at the outlet of the channel, the mean temperature of the melt decreases, while the profile shows a maximum at the channel center. These observations result mainly of the low thermal conductivity of the melt and of the heat losses through the non-heated faces of the extrusion die. It is observed that

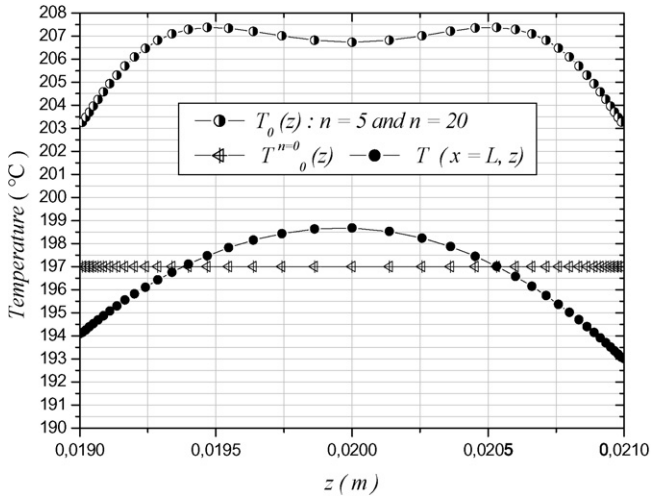

Fig. 14. Estimated inlet and outlet temperature profiles for PE Dowlex 2042^{E}. $P_{melt} = 20$ MPa, $S_{p,w} \neq 0$.

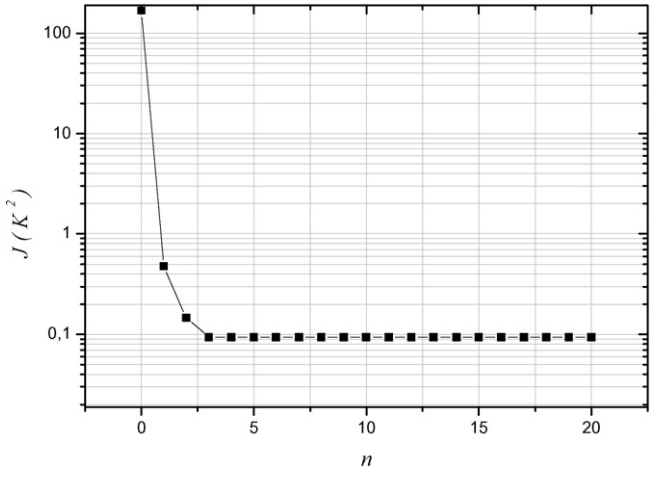

Fig. 15. Least square criterion $J(T_0(z))$, $S_{p,w} \neq 0$.

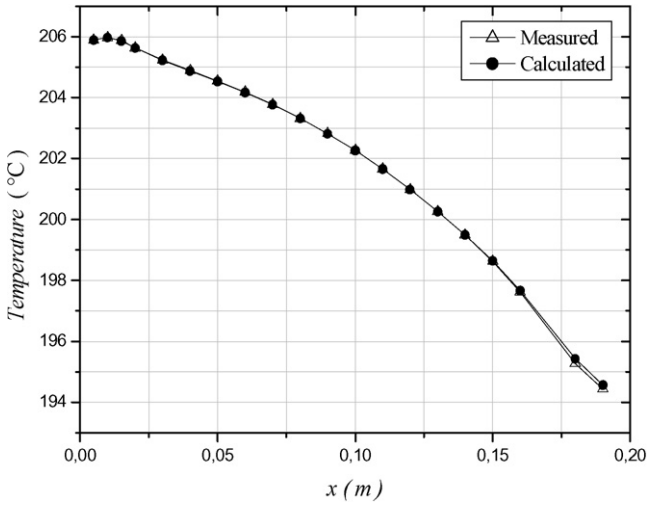

Fig. 16. Measured and calculated temperatures for PE Dowlex 2042^{E} $P_{melt} = 20$ MPa, $S_{p,w} \neq 0$.

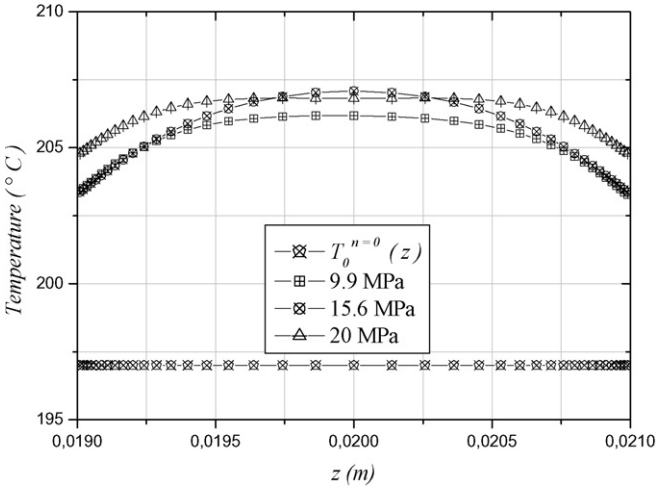

Fig. 17. Estimated inlet temperatures for PE Dowlex 2042^{E}.

when the number of iterations increases, the final value of the least square criterion decreases (Fig. 15) and a reasonably inlet temperature solution is obtained after five iterations. Although the optimal number of iterations is difficult to be determined a priori, the plot of the iterative process, Figs. 15–16, confirms the efficiency of the CGM and suggests that the optimal number of iterations is around 5, when the least square criterion J is close to the expected value: $J = N_s\sigma^2$, which leads here to $\sigma^2 \approx 0.09/40 \Rightarrow \sigma \approx 0.047\,^{\circ}\mathrm{C}$. This value of the standard deviation of the measurement noise is quite correct. The inlet temperature profile estimated at the iteration numbers 5 and 20 remains unchanged.

5.1.2. *Effect of the flow rate on the inlet temperature* ($S_{p,w}(x, z, T) \neq 0$)

In these tests, we varied the pressure drop ΔP (flow rate) along the channel die by increasing the screw rotation velocity. Fig. 5 shows the influence of the pressure drops on the temperature near the heating-plate. The temperature is maximal at the die inlet (the curves are relatively grouped) and then decreases slightly. It was thought that the differences in inlet melt temperature could be explained in connection with the flow rate in the channel. It is widely accepted that an increase in outlet melt temperature is caused by shear heating effect. Our objective is to include/understand the thermal state of the die. For this we have to study the influence of the flow rate on the estimated temperature. Fig. 17 shows the estimated inlet temperature profile in accordance with the flow rate ($\Delta P = 9.9$ MPa, 15.6 MPa and 20 MPa). When the pressure drop increases, more melted polymer can flow through the channel die and that can cause internal heating that changes the average temperature and thus the viscosity. Analysis shows, however, that this effect tends to increase the outlet temperature even more rapidly with flow rate (Fig. 18). Figs. 19–20 show the comparison between the measured and calculated temperature and the evolution of the least square criterion for three operating conditions: 9.9–15.6 and 20 MPa. The evolution of the least square criterions is similar. After five iterations, the criterion remains constant. The standard deviation of the measurement noise for these cases is given by: $\sigma_{9.9\ \mathrm{MPa}} = 0.1\,^{\circ}\mathrm{C}$, $\sigma_{15.6\ \mathrm{MPa}} = 0.07\,^{\circ}\mathrm{C}$, $\sigma_{20\ \mathrm{MPa}} = 0.047\,^{\circ}\mathrm{C}$. Processing conditions, which in turn affect

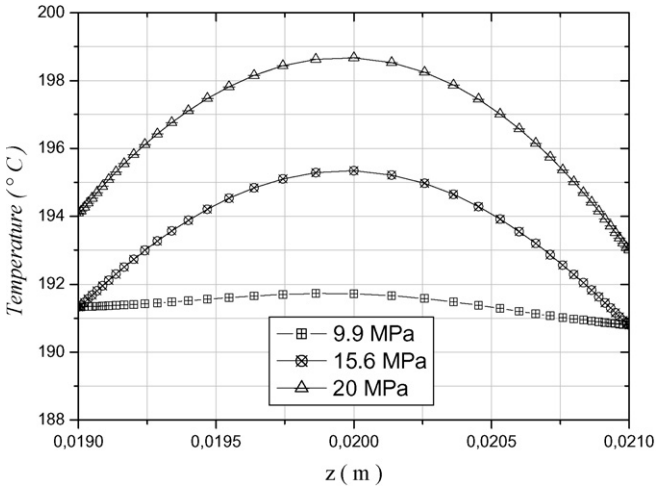

Fig. 18. Calculated outlet temperatures for PE Dowlex 2042^{E}.

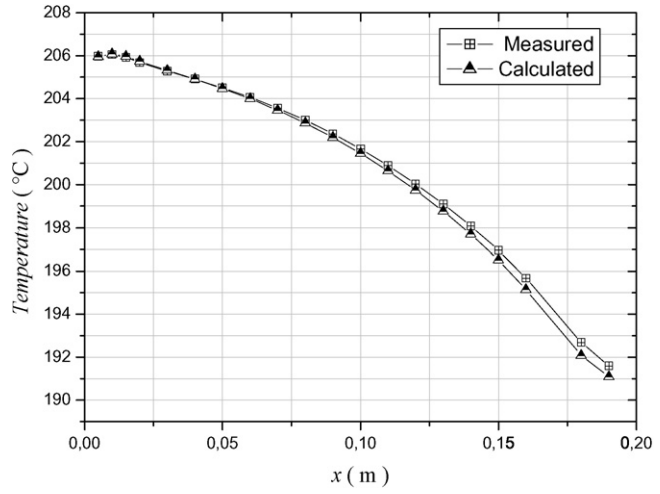

Fig. 19. Measured and calculated temperatures for PE Dowlex 2042^{E} $P_{melt} = 9.9$ MPa; $S_{p,w} \neq 0$.

the estimated inlet temperature profile, play an important role in changing the rheological properties of the extruded melt and the die thermal state.

5.1.3. Nusselt number in the channel die

The usual definition of Nusselt number is $Nu(x) = h(x)D_h/\lambda_p$ where λ_p is the thermal conductivity. According to the expression of the heat transfer coefficient, the Nusselt number can be written in the form: $Nu(x) = \frac{\lambda_w D_h}{\lambda_p(T_{p,\sup,\inf} - T_b)(x)} \times (\partial T/\partial z)_{z=h}$. Where: $T_m = \frac{1}{u_m h}\int_0^h uT(x,y)\,dz$ is the bulk temperature, $D_h = 4(l.h)/2(h+l)$, is the hydraulic diameter. In order to calculate $Nu(x)$ only from experimental data, in the case of non-uniform inlet and wall temperature, inlet temperature profile were estimated using inverse method. Heat flux is calculated using the measuring temperatures at the polymer/die interface and the wall temperatures $T_{p,\sup,\inf}$ (Fig. 7). Fig. 21 represents the local Nusselt number for two different Cameron numbers ($Ca = L\lambda_p/\rho_p C_{pp} u_m h^2$: $Ca = 0.56$–0.85) and clearly indicates that we are in a situation where the thermal field is not established and far from an asymptotic behaviour

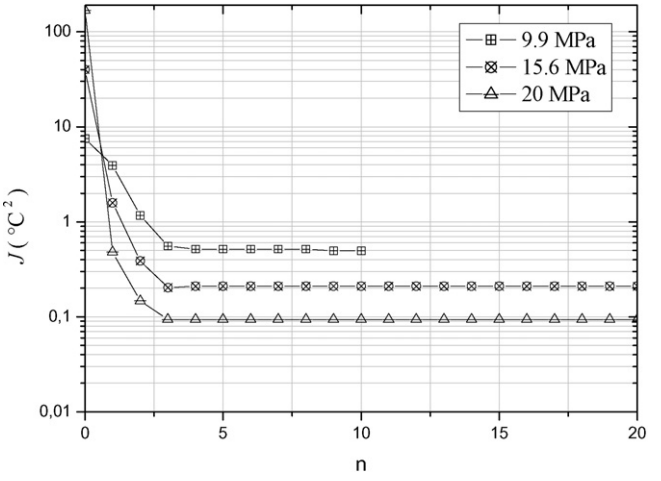

Fig. 20. Least square criterion vs. iterations.

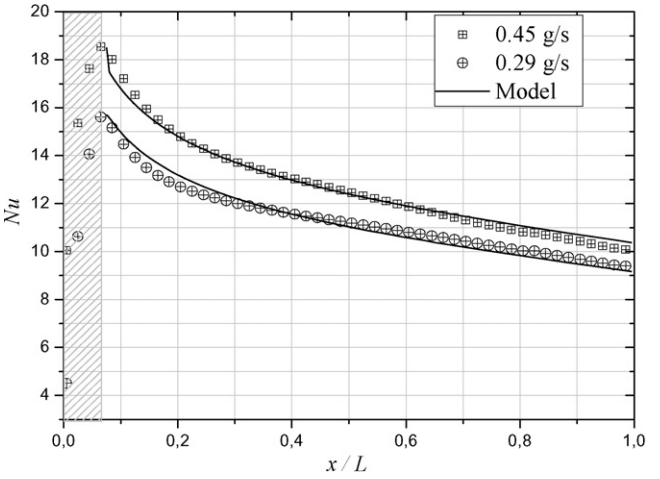

Fig. 21. Local Nusselt number for two-flow rates.

($x \geqslant 0.015$ m). We can account for the variations of the axial position and flow rate by using the usual dimensionless variable $\xi = 2x/D_h P_e$ (Fig. 22). Note that the Peclet number ($P_e = \rho_p u_m D_h C_{pp}/\lambda_p$) does not contain information about rheological behaviour of polymer and that this analysis remains reasonable for all the values of the die inlet temperatures. On the other hand, it should be noted that the variations in the Nusselt number remain dependent on the estimated inlet temperature and the bulk temperature (Fig. 23). The variation of the experimental Nusselt numbers can be reasonably approached using the dimensionless axial abscissa ξ. This correlation is based on the work of Levêque [24] $Nu(x) = 1.233(Gz)^{1/3}(Gz = P_e/xD_h)$ that we multiply by two correcting factors. The first one describes the non-Newtonian character of the fluid $\Pi = (2n + 1/3n)^{1/3}$ (Pigford 1955). The second one, $(K(T_m)/K(T_w))^e = (\exp(bT_m)/\exp(bT_w))^e$, takes into account the wall temperature variations and the temperature dependence of the viscosity. Hence we propose a simple correlation $Nu(x) = c \times \Pi(\frac{2x}{Dh.P_e})^d(\frac{K(T_m)}{K(T_w)})^e$ seem to be acceptable in our experimental range with the following parameters: $c = 15.56$, $d = -0.19$ and $e = 4.45$.

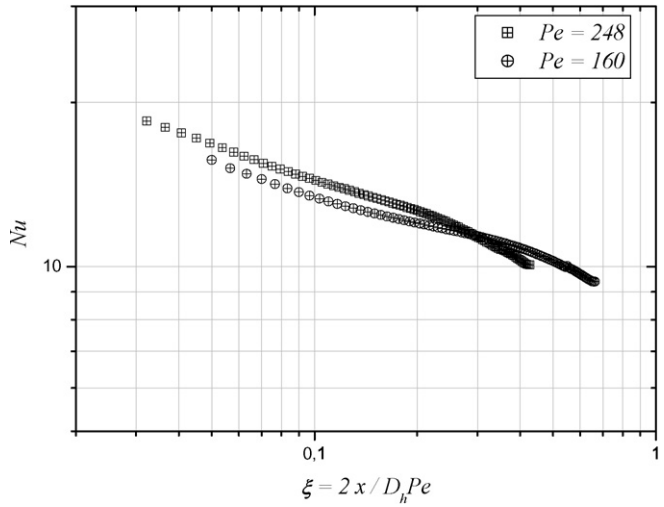

Fig. 22. Nusselt number versus ξ and P_e.

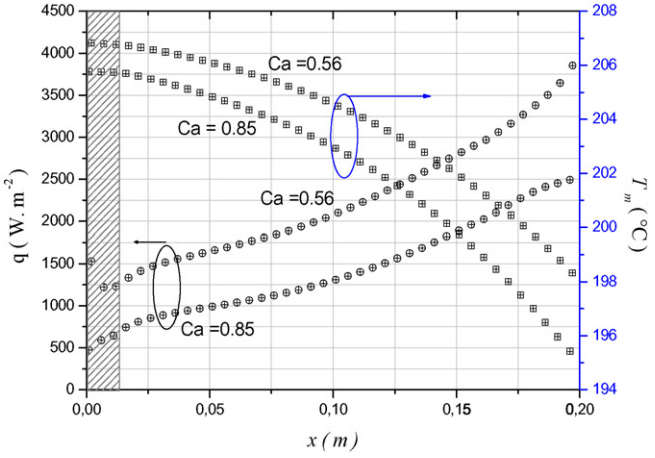

Fig. 23. Distribution of heat flux and bulk temperature.

6. Conclusions

An inverse algorithm and a specific apparatus have been used to determine the inlet temperature profile of the melted polymer from the temperature data measured in the solid wall of the extrusion die. This experimental and numerical study show the effect of the pressure drop combined with the viscous dissipation on the temperature profile along the channel die and the Nusselt number at the polymer/wall interface. The reconstructed temperature profile without lateral heat losses is not attainable from a physical point of view. A reasonable profile was obtained when we take into account the heat losses ($S_{p,w}(x, z, T) \neq 0$) in the mathematical modelling. The local Nusselt number allows a better understanding of the impact of inlet temperature and flow rate on the thermal state of the die. This work has shown that it is necessary to take into account the interaction between the thermal and dynamic field to determine the local values of the heat transfer coefficient.

References

[1] Z. Tadmor, C.G. Gogos, Principles of Polymer Processing, Wiley, New York, 1979.
[2] J.F. Agassant, P. Avenas, P. Sergent, P. Carreau, Polymer Processing Principles and Modeling, Hanser Publishers, Munich, 1991.
[3] F.C. Liu, M.N. Özisik, Estimation of inlet temperature profile in laminar duct flow, Inverse Probl. Engrg. 3 (1996) 131–141.
[4] J.C. Bokar, M.N. Özisik, Inverse analysis for estimating the time varying inlet temperature in laminar flow inside a parallel plate duct, Int. J. Heat Mass Transfer 38 (1995) 39–45.
[5] C.H. Huang, M.N. Özisik, Inverse problem of determining unknown wall heat flux in laminar flow trough a parallel plate, Numer. Heat Transfer 21 (1992) 55–70.
[6] H.A. Machado, H.R.B. Orlande, Inverse problem for estimating the heat flux to a non-Newtonian fluid in a parallel plate channel, J. Brazilian Soc. Mech. Sci. 20 (1998) 51–61.
[7] P.T. Hsu, C.K. Chen, Y.T. Yang, A 2-D inverse method for simultaneous estimation of the inlet temperature and wall heat flux in laminar circular duct flow, Numer. Heat Transfer 34 (1989) 731–745.
[8] C.-H. Huang, W.-C. Chen, A three-dimensional inverse forced convection problem in estimating surface heat flux by conjugate gradient method, Int. J. Heat Mass Transfer 43 (2000) 3171–3181.
[9] I. Gegadze, Y. Jarny, An inverse heat transfer problem for restoring the temperature field in a polymer melt flow through a narrow channel, Int. J. Thermal Sci. 41 (2002) 528–535.
[10] K.T. Nguyen, M. Prystay, An inverse method for estimation of the initial temperature profile and its evolution in polymer processing, Int. J. Heat Mass Transfer 42 (1998) 1969–1978.
[11] M. Karkri, Heat transfer in steady polymer flow through an extrusion die: Thermal metrology and inverse method, PhD Thesis, University of Nantes, 2004.
[12] H.C. Brinkman, Heat effects in capillary flow I, Appl. Sci. Res. A 2 (1951) 120–124.
[13] O. Aydm, Effects of viscous dissipation on the heat transfer in a forced pipe flow. Part 1, both hydrodynamically and thermally fully developed flow, Energy Conversion Management 46 (2005) 757–769.
[14] R.K. Shah, A.L. London, Laminar flow forced convection in ducts, Adv. Heat Transfer (suppl. 1) Academic Press, New York, 1978.
[15] R.K. Shah, M.S. Bhatti, Laminar convective heat transfer in ducts, in: S. Kakaç, R.K. Shah, W. Aung (Eds.), Handbook of Single-Phase Convective Heat Transfer, Wiley, New York, 1987.
[16] J.P. Hartnett, M. Kostic, Heat transfer to Newtonian and non-Newtonian fluids in rectangular ducts, Adv. Heat Transfer 19 (1989) 247–356.
[17] S.X. Gao, J.P. Hartnett, Analytical Nusselt number predictions for slug flow in rectangular duct, Int. Commun. Heat Mass Transfer 20 (1993) 751–760.
[18] A. Barletta, E. Zanchini, Forced convection in the thermal entrance region of a circular duct with slug flow and viscous dissipation, Int. J. Heat Mass Transfer 40 (5) (1997) 1181–1190.
[19] T. Jurkowski, Mise en œuvre d'une méthode et réalisation d'un appareillage de mesure de la conductivité thermique d'un polymère, PhD, Thesis, University of Nantes, 1993.
[20] F. Kreith, R.F. Boehm, et al., Heat and Mass Transfer, in: F. Kreith (Ed.), Mechanical Engineering Handbook, CRC Press LLC, Boca Raton, 1999.
[21] M. Karkri, Y. Jarny, P. Mousseau, Paper presented at the International Symposium of Inverse Problem Design and Optimisation, Rio de Janerio, Brazil, 2004.
[22] M. Karkri, Y. Jarny, P. Mousseau, Inverse heat transfer analysis in a polymer melt flow within an extrusion die, IPSE 13 (4) (2004) 355–375.
[23] M. Karkri, Y. Jarny, P. Mousseau, R. Deterre, Thermique de l'écoulement d'un polymère pseudoplastique, in: Acte du congrès SFT, Elsevier, 2003, pp. 667–672.
[24] M.A. Levêque, Les lois de la transmission de la chaleur par convection, Annales Mines (1928) 201–203.